

# Effect of impurities in high-symmetry lattice positions on the local density of states and conductivity of graphene

F. M. D. Pellegrino,<sup>1,2,3</sup> G. G. N. Angilella,<sup>1,2,3,4,\*</sup> and R. Pucci<sup>1,4</sup>

<sup>1</sup>*Dipartimento di Fisica e Astronomia, Università di Catania,  
Via S. Sofia, 64, I-95123 Catania, Italy*

<sup>2</sup>*Scuola Superiore di Catania, Via S. Nullo, 5/i, I-95123 Catania, Italy*

<sup>3</sup>*INFN, Sez. Catania, I-95123 Catania, Italy*

<sup>4</sup>*CNISM, UdR Catania, I-95123 Catania, Italy*

(Dated: December 5, 2018)

Motivated by quantum chemistry calculations, showing that molecular adsorption in graphene takes place on preferential sites of the honeycomb lattice, we study the effect of an isolated impurity on the local electronic properties of a graphene monolayer, when the impurity is located on a site-like, bond-like, or hollow-like position. We evaluate the local density of states (LDOS) as a function of energy on the impurity and on its neighboring sites, as well as in reciprocal space, at an energy corresponding to a bound state, in the three cases of interest. The latter study may be relevant to interpret the results of Fourier transformed scanning tunneling spectroscopy, as they show which states mostly contribute to impurity-induced variations of the LDOS. We also estimate, semi-analytically, the dependence of the condition for having a low-energy bound state on the impurity potential strength and width. Such results are then exploited to obtain the quasiparticle lifetime and the static conductivity in graphene in the dilute impurity limit. In particular, we recover a sublinear dependence of the conductivity on the carrier concentration as a generic impurity effect.

PACS numbers: 71.23.-k, 73.23.-b, 81.05.Uw

## I. INTRODUCTION

Graphene is the two-dimensional allotrope of carbon, which is characterized by a honeycomb lattice. Despite its structural simplicity, only recently it has been obtained in laboratory<sup>1,2,3</sup>, thus giving rise to a tremendous outburst of research activity, both among experimentalists and theoreticians. Its remarkable electronic properties, largely due to its reduced dimensionality, and its relatively high degree of symmetry, make graphene an ideal candidate for applications in micro and nanoelectronics. In particular, it has been recently suggested that charging can be controlled at the atomic level, thereby enabling one to tailor some of the magnetic properties of the system<sup>4</sup>. On the other hand, its linear quasiparticle dispersion relation suggests an analogy between the low-energy excitations in graphene and relativistic massless particles, obeying Dirac-Weyl equation, thus allowing the study of relativistic effects in a condensed matter system<sup>5,6</sup>.

Since most of the intriguing physical properties of graphene stem from its perfect crystal lattice, it is of interest to study how some of these are affected by the presence of localized impurities. It is well-known that disorder can significantly affect the electronic properties of graphene, especially when the chemical potential traverses the Dirac points. This can be brought about not only by impurities<sup>7,8,9</sup>, but also by topological defects<sup>10</sup>, edges<sup>11</sup>, substrate corrugations<sup>12</sup>, and ripples<sup>13</sup>.

Isolated short-range impurities have been shown to modify the local single-particle electronic properties of graphene, such as the local density of states

(LDOS)<sup>7,9,11,14</sup>, and can induce Friedel oscillations<sup>8</sup>. The role of strength, width and concentration of impurities in altering the local energy spectrum has been studied theoretically<sup>11,15</sup>. The relevance of special symmetries and how they manifest themselves in the scattering around impurities has been emphasized in Ref. 16. Moreover, the study of the impurity effects on the LDOS is relevant to analyze the experimental results of scanning tunneling microscopy (STM)<sup>12,17,18</sup>, and can elucidate the role of correlations in the electron liquid in graphene. In particular, it has been suggested that Fourier transformed scanning tunneling spectroscopy (FTSTS) results can also be instrumental to identify experimentally monolayer and bilayer graphene<sup>9,19</sup>.

Disorder is also known to affect considerably the transport properties of graphene. In particular, the presence of disorder may explain the finite value of the conductivity in pure graphene<sup>20,21</sup>. In the case of graphene on a substrate, an inhomogeneous potential distribution may be brought about by charged impurities located close to the substrate surface. At low electron or hole concentration, this may induce sizeable spatial fluctuations of the carrier concentration, and may therefore justify a nonzero conductivity, even in the absence of any gate potential<sup>21</sup>. This has been experimentally verified using a scanning single-electron transistor<sup>13</sup>. Such a regime of inhomogeneity persists beyond neutrality, and characterizes also suspended graphene samples before annealing<sup>22</sup>. After annealing, the conductivity displays a sublinear dependence on carrier concentration around zero doping, which may be due to short-range impurities, such as point defects<sup>23,24,25</sup>.

In this paper, we will be mainly concerned with the effects on the LDOS and on the conductivity of graphene due to single or distributed impurities located in a high-symmetry position of the honeycomb lattice. These include the sites of the direct lattice, the position midway two neighboring carbon atoms, and the center of the hexagon plaquettes. Such positions have been extensively studied also within quantum chemical calculations, as they are expected to be favored in the adsorption of hydrogen, water, and other simple molecules<sup>26</sup>.

After reviewing the formalism for a single localized impurity in graphene in Sec. II, we will present our results for the LDOS in the presence of a single impurity, either in the site-like, bond-like, or hollow-like configuration (Sec. III). Our results include the energy dependence of the LDOS on the impurity site and its nearest neighbors, and the reciprocal lattice structure of the LDOS close to a resonance. Then, in Sec. IV, we will generalize the above results in the case of many impurities, in the dilute limit, within the full Born approximation. In particular, we shall be interested in the case in which all impurities are located in a preferential class of lattice sites. We will derive the LDOS in reciprocal space in the case of many impurities, and discuss the dependence of the quasiparticle lifetime on the impurity concentration. Finally, it will be shown that, close to a low-energy resonance, disorder induces a sublinear dependence of the conductivity on the carrier concentration, and that such an effect is rather insensible to the impurity concentration, albeit in the dilute limit. We summarize our results in Sec. V.

## II. MODEL

We begin by reviewing the tight-binding approximation and the  $T$ -matrix formalism for a single non-magnetic impurity in graphene<sup>27</sup>. Within the tight-binding approximation, a graphene monolayer in the presence of a single impurity localized at position  $\mathbf{x}$  will be described by the Hamiltonian

$$H = \sum_{\mathbf{k}\lambda} \xi_{\mathbf{k}\lambda} c_{\mathbf{k}\lambda}^\dagger c_{\mathbf{k}\lambda} + V_0 \Psi^\dagger(\mathbf{x}) \Psi(\mathbf{x}). \quad (1)$$

Here,  $c_{\mathbf{k}\lambda}^\dagger$  ( $c_{\mathbf{k}\lambda}$ ) is a creation (annihilation) operator for a quasiparticle with wavevector  $\mathbf{k}$  within the first Brillouin zone and band index  $\lambda = 1, 2$ ,  $\xi_{\mathbf{k}\lambda} = E_{\mathbf{k}\lambda} - \mu$  is the tight-binding dispersion relation for band  $\lambda$ , measured with respect to the chemical potential  $\mu$ , and  $V_0$  is a measure of the strength of the impurity potential. Expanding the field operators  $\Psi^\dagger(\mathbf{x})$ ,  $\Psi(\mathbf{x})$  appearing in the impurity potential with respect to the tight-binding basis states, one finds

$$H = \sum_{\mathbf{k}\lambda} \xi_{\mathbf{k}\lambda} c_{\mathbf{k}\lambda}^\dagger c_{\mathbf{k}\lambda} + \sum_{\mathbf{k}\mathbf{k}'\lambda\lambda'} V_{\lambda\lambda'}(\mathbf{k}, \mathbf{k}') c_{\mathbf{k}\lambda}^\dagger c_{\mathbf{k}'\lambda'}, \quad (2)$$

where

$$V_{\lambda\lambda'}(\mathbf{k}, \mathbf{k}') = V_0 \psi_{\mathbf{k}\lambda}^*(\mathbf{x}) \psi_{\mathbf{k}'\lambda'}(\mathbf{x}), \quad (3)$$

and  $\psi_{\mathbf{k}\lambda}(\mathbf{x})$  is the Bloch wavefunction employed in the tight-binding diagonalization of the pure sector of the Hamiltonian.

### A. Tight-binding approximation

For the sake of completeness, we briefly review the main features of the tight binding approximation employed in the present work. Graphene is characterized by a honeycomb lattice, with basis vectors  $\mathbf{a}_1 = a(3, \sqrt{3})/2$  and  $\mathbf{a}_2 = a(3, -\sqrt{3})/2$ , where  $a = 0.142$  nm is the C–C distance<sup>3</sup>. This is equivalent to two interpenetrating  $A$  and  $B$  triangular sublattices, with nearest neighbor sites connected by the vectors  $\delta_1 = a(1, \sqrt{3})/2$ ,  $\delta_2 = a(1, -\sqrt{3})/2$ ,  $\delta_3 = a(-1, 0)$ . Correspondingly, the first Brillouin zone in the reciprocal lattice is an hexagon with vertices in the so-called Dirac points,  $\mathbf{K} = \frac{2\pi}{3a}(1, \frac{\sqrt{3}}{3})$ ,  $\mathbf{K}' = \frac{2\pi}{3a}(1, -\frac{\sqrt{3}}{3})$ .

A suitable choice within the standard tight-binding approximation consists in retaining hopping and overlap terms between nearest neighbor sites<sup>28</sup>. This gives rise to the two bands

$$E_{\mathbf{k}\lambda} = \frac{\pm t |\gamma_{\mathbf{k}}|}{1 \mp s |\gamma_{\mathbf{k}}|}, \quad (4)$$

where the bottom and top signs apply to the valence band, with  $\lambda = 1$ , and conduction band, with  $\lambda = 2$ , respectively. In Eq. (4),  $t = 2.8$  eV and  $s = 0.07$  are the nearest neighbor hopping and overlap parameters, respectively<sup>29</sup>, and

$$\gamma_{\mathbf{k}} = \sum_{\ell=1}^3 e^{i\mathbf{k}\cdot\delta_\ell} \quad (5)$$

is the usual (complex) structure factor in momentum space. In the limit  $s = 0$ , one recovers the symmetry between valence and conduction bands,  $E_{\mathbf{k}\lambda} = \pm t |\gamma_{\mathbf{k}}|$ .

One has still a choice to fix the functional form of the Bloch wavefunctions that define the basis set implied in the tight binding approximation. These are linear combination of tightly bound atomic functions, and will therefore be termed pseudoatomic wavefunctions in the following. The approximation of using pseudoatomic wavefunctions with a finite extension, while retaining a localized impurity potential, allows one to treat exactly also the case in which a short-range impurity is located in an out-of-lattice position, as is the case of hollow-like impurities addressed to below (Sec. III C). Due to the two-dimensionality of the graphene sheet, we can safely neglect their extension along the axis orthogonal to the graphene plane,  $z$  say.

One possible choice is such that its square modulus is a normalized gaussian<sup>30</sup>

$$\phi_g(\mathbf{r}) = \frac{1}{2\sqrt{3}\pi} \frac{Z_g}{a} \exp(-\rho_g^2/24), \quad (6)$$

where  $\rho_g = Z_g r/a$ , and  $Z_g$  can be used to tune the spatial extension of the wavefunction, characterized by an average radius  $\bar{r}_g = \langle x^2 + y^2 \rangle_g^{1/2} = 2\sqrt{3}a/Z_g$ .

Another possible choice is such that its square modulus is a normalized combination of modified Bessel functions of second kind<sup>31</sup>

$$\phi_b(\mathbf{r}) = \frac{1}{4\sqrt{\pi}} \frac{Z_b}{a} \sqrt{2\rho_b K_1(\rho_b) + \rho_b^2 K_0(\rho_b)}, \quad (7)$$

where  $\rho_b = Z_b r/a$ , and  $Z_b$  is again a parameter related to the spatial extension. Like the gaussian pseudoatomic wavefunction, Eq. (6), also Eq. (7) has a bell-shaped behavior, but decays more slowly,  $\phi_b(\mathbf{r}) \sim \rho_b^{3/4} \exp(-\rho_b)$ , for  $\rho_b \gg 1$ . The expectation value of any cylindrically symmetric function with respect to Eq. (7) is the same as the expectation value with respect to the  $2p_z$  hydrogenic wavefunction with atomic number  $Z_b$ . In particular, the average radius is similarly given by  $\bar{r}_b = \langle x^2 + y^2 \rangle_b^{1/2} = 2\sqrt{3}a/Z_b$ .

In both cases, the parameters are fixed by the condition that the nearest neighbor overlap integral yields<sup>29</sup>  $s = 0.07$ , so that  $Z_g = 11.2$  and  $Z_b = 12.8$ . In the case of a single impurity, we have numerically verified that all results do not qualitatively depend on the particular choice of the pseudoatomic wavefunction, and that any quantitative difference is within graphical resolution. This is because the impurity effects considered here depend mainly on the short-distance behavior of  $\phi(\mathbf{r})$ . Therefore, in this paper we have chosen to present results obtained with the gaussian choice for the pseudoatomic wavefunctions, Eq. (6). In terms of these, the Bloch wavefunction on which the tight-binding approximation is based is

$$\psi_{\mathbf{k}\lambda}(\mathbf{r}) = \frac{1}{\sqrt{N}} \sum_j \phi(\mathbf{r} - \mathbf{R}_j^\lambda) e^{i\mathbf{k}\cdot\mathbf{R}_j^\lambda}, \quad (8)$$

where  $\mathbf{R}_j^\lambda$  are vectors of the  $\lambda = A$  and  $B$  sublattices, respectively.

Let  $\psi_{\mathbf{k}\mu}$  ( $\mu = A, B$ ) denote the Bloch wavefunctions in the sublattice representation. These are then related to the Bloch wavefunctions  $\psi_{\mathbf{k}\lambda}$  ( $\lambda = 1, 2$ ) in the band representation, Eq. (8), by the unitary transformation

$$\psi_{\mathbf{k}\lambda} = \sum_{\mu=A,B} U_{\lambda\mu}(\mathbf{k}) \psi_{\mathbf{k}\mu}, \quad (9)$$

where  $U_{\lambda\mu}(\mathbf{k})$  is the generic element of the matrix

$$U(\mathbf{k}) = \frac{1}{\sqrt{2}} \begin{pmatrix} 1 & -1 \\ e^{-i\theta_{\mathbf{k}}} & e^{-i\theta_{\mathbf{k}}} \end{pmatrix}, \quad (10)$$

and

$$e^{i\theta_{\mathbf{k}}} = -\frac{\gamma_{\mathbf{k}}}{|\gamma_{\mathbf{k}}|}, \quad (11)$$

with  $\gamma_{\mathbf{k}}$  defined in Eq. (5).

## B. $T$ -matrix formalism

We then introduce the finite-temperature Green's functions

$$\mathcal{G}_{\lambda\lambda'}(\mathbf{k}, \mathbf{k}', \tau) = -\langle T_\tau [c_{\mathbf{k}\lambda}(\tau) c_{\mathbf{k}'\lambda'}^\dagger(0)] \rangle, \quad (12)$$

where  $\langle \dots \rangle$  is a quantum statistical average with respect to  $H$  at temperature  $T$ , and  $T_\tau$  denotes ordering with respect to the imaginary time  $\tau$ . Making use of the fermionic Matsubara frequencies  $\hbar\omega_n = (2n+1)\pi k_B T$ , where  $\hbar$  is Planck's constant and  $k_B$  is Boltzmann's constant, one finds the usual Dyson's equation

$$\mathcal{G}_{\lambda\lambda'}(\mathbf{k}, \mathbf{k}', i\omega_n) = \delta_{\lambda\lambda'} \delta_{\mathbf{k}\mathbf{k}'} \mathcal{G}_\lambda^0(\mathbf{k}, i\omega_n) + \sum_{\mathbf{q}\lambda''} \mathcal{G}_{\lambda\lambda''}(\mathbf{k}, \mathbf{q}, i\omega_n) V_{\lambda''\lambda'}(\mathbf{q}, \mathbf{k}') \mathcal{G}_{\lambda'}^0(\mathbf{k}', i\omega_n), \quad (13)$$

where  $\mathcal{G}_\lambda^0(\mathbf{k}, i\omega_n) = (i\omega_n - \xi_{\mathbf{k}\lambda})^{-1}$  is the Green's function of the pure system. Dyson's equation (13) can be solved iteratively by exploiting the fact that the impurity potential is factorizable in momentum space (see Appendix A). One finds

$$\mathcal{G}_{\lambda\lambda'}(\mathbf{k}, \mathbf{k}', i\omega_n) = \delta_{\lambda\lambda'} \delta_{\mathbf{k}\mathbf{k}'} \mathcal{G}_\lambda^0(\mathbf{k}, i\omega_n) + \mathcal{G}_\lambda^0(\mathbf{k}, i\omega_n) T_{\lambda\lambda'}(\mathbf{x}; \mathbf{k}, \mathbf{k}', i\omega_n) \mathcal{G}_{\lambda'}^0(\mathbf{k}', i\omega_n), \quad (14)$$

where

$$T_{\lambda\lambda'}(\mathbf{x}; \mathbf{k}, \mathbf{k}', i\omega_n) = \frac{1}{N} \frac{V_0 \check{\psi}_{\mathbf{k}\lambda}^*(\mathbf{x}) \check{\psi}_{\mathbf{k}'\lambda'}(\mathbf{x})}{1 - V_0 \mathcal{G}^0(\mathbf{x}, \mathbf{x}, i\omega_n)} \quad (15)$$

is the generic element of the  $T$ -matrix,  $\check{\psi}_{\mathbf{k}\lambda}(\mathbf{x}) = \sqrt{N} \psi_{\mathbf{k}\lambda}(\mathbf{x})$  is a rescaled basis function, and

$$\mathcal{G}^0(\mathbf{r}, \mathbf{r}', i\omega_n) = \frac{1}{N} \sum_{\mathbf{q}\lambda'} \check{\psi}_{\mathbf{q}\lambda'}(\mathbf{r}) \mathcal{G}_{\lambda'}^0(\mathbf{q}, i\omega_n) \check{\psi}_{\mathbf{q}\lambda'}^*(\mathbf{r}'). \quad (16)$$

Eq. (14) shows that the correction due to a single localized impurity vanishes as  $1/N$  in the thermodynamic limit,  $N \rightarrow \infty$ . Going back to real space by means of Eq. (16), one finds the imaginary-time Green's function at position  $\mathbf{r}$

$$\mathcal{G}(\mathbf{r}, \mathbf{r}, i\omega_n) = \mathcal{G}^0(\mathbf{r}, \mathbf{r}, i\omega_n) + \frac{V_0 \mathcal{G}^0(\mathbf{r}, \mathbf{x}, i\omega_n) \mathcal{G}^0(\mathbf{x}, \mathbf{r}, i\omega_n)}{1 - V_0 \mathcal{G}^0(\mathbf{x}, \mathbf{x}, i\omega_n)}. \quad (17)$$

In what follows, we shall be interested in the local density of states (LDOS)  $\rho(\mathbf{r}, \omega)$ , which is experimentally accessible through STM measurements<sup>12,17,18</sup>, and is related to the imaginary part of the analytically continued Green's function through

$$\rho(\mathbf{r}, \omega) = -\frac{1}{\pi} \text{Im} G(\mathbf{r}, \mathbf{r}, \omega), \quad (18)$$

where  $G(\mathbf{r}, \mathbf{r}, \omega) = \mathcal{G}(\mathbf{r}, \mathbf{r}, i\omega_n \rightarrow \omega + i0^+)$ . It is straightforward to observe that the chemical potential enters  $G(\omega)$  only as an additive constant to  $\omega$ . Therefore, we

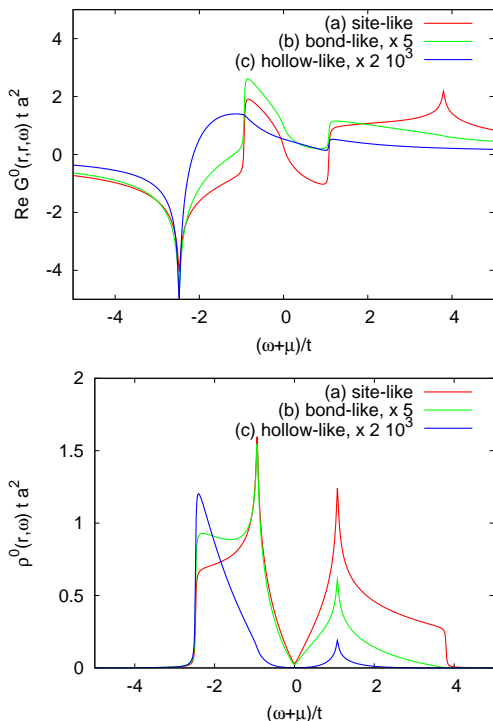


FIG. 1: (Color online) Real part of the unperturbed Green's function,  $\text{Re } G^0(\mathbf{x}, \omega)$  (top panel), and unperturbed LDOS,  $\rho^0(\mathbf{x}, \omega) = -\pi^{-1} \text{Im } G^0(\mathbf{x}, \omega)$  (bottom panel), for the three cases of interest: (a) site-like impurity ( $\mathbf{x} = \mathbf{0}$ ), (b) bond-like impurity ( $\mathbf{x} = \delta_3/2$ ), (c) hollow-like impurity ( $\mathbf{x} = -\delta_3$ ). It should be noticed that the latter two cases have been scaled by the factors indicated in the caption.

can set hereafter  $\mu = 0$ , thereby neglecting any contribution arising from chemical or electrical doping, *e.g.* through a gate voltage.

Inspection of Eqs. (17) and (18) shows that the LDOS on the impurity position ( $\mathbf{r} = \mathbf{x}$ ) is given by

$$\rho(\mathbf{x}, \omega) = \frac{\rho^0(\mathbf{x}, \omega)}{[1 - V_0 \text{Re } G^0(\mathbf{x}, \mathbf{x}, \omega)]^2 + [\pi V_0 \rho^0(\mathbf{x}, \omega)]^2}, \quad (19)$$

with  $\rho^0(\mathbf{x}, \omega)$  denoting the LDOS at position  $\mathbf{r} = \mathbf{x}$  in the pure case. In the limit of a vanishing unperturbed LDOS,  $\rho^0(\mathbf{x}, \omega) \rightarrow 0$ , one has  $\rho(\mathbf{x}, \omega) \rightarrow V_0^{-1} \delta[1 - V_0 \text{Re } G^0(\mathbf{x}, \mathbf{x}, \omega)]$ . Such a circumstance is *e.g.* realized below the valence band,  $\omega \leq \omega_{\perp} \approx -2.48t$ , or above the conduction band,  $\omega \geq \omega_{\top} \approx 3.80t$ . Direct inspection of  $\text{Re } G^0(\mathbf{x}, \mathbf{x}, \omega)$  as a function of  $\omega$  (Fig. 1) leads to the existence of a bound state outside the two bands, for a wide range of potential strengths  $V_0$ . In particular, a bound state at  $\omega < 0$  may be formed below the valence band only for some  $V_0 < 0$ , or above the conduction band for  $V_0 > 0$ , the energy of such a bound state moving farther from the bands, as  $|V_0|$  increases.

For future reference, it is also of interest to quote the expression of the LDOS close to a bound state in recip-

rocal space, which reads

$$\begin{aligned} \rho_{\lambda}(\mathbf{k}, \omega) &= -\frac{1}{\pi} \text{Im } G_{\lambda}(\mathbf{k}, \omega) \\ &= \frac{V_0}{N} \frac{|\check{\psi}_{\mathbf{k}\lambda}(\mathbf{x})|^2}{|\omega - \xi_{\lambda\mathbf{k}}|^2} \delta[1 - V_0 \text{Re } G^0(\mathbf{x}, \mathbf{x}, \omega)] \end{aligned} \quad (20)$$

In other words, Eq. (20) applies to states with a vanishing unperturbed LDOS, *i.e.* to frequencies  $\omega$  such that  $\rho^0(\mathbf{k}, \omega) = 0$  for all wavevectors  $\mathbf{k}$  in the 1BZ. This corresponds to  $\omega < \omega_{\perp}$ ,  $\omega = 0$ , and  $\omega > \omega_{\top}$ .

### III. SINGLE IMPURITY

In what follows, we shall analyze the effect on the LDOS, Eq. (18), due to a single impurity localized in several high-symmetry positions of the primitive cell in the graphene honeycomb lattice. These include an *A* or *B* site, usually occupied by a carbon atom (site-like impurity), the position midway between an *A* and *B* site (bond-like impurity), and the position at the center of an hexagon plaquette (hollow-like impurity).

#### A. Site-like impurities

Let us start by considering an impurity located on an *A* or *B* site (say  $\mathbf{x} = \mathbf{0}$ , for definiteness). Such an impurity preserves the  $D_{3h}$  symmetry. This could be used to model a hydrogen impurity adsorbed on a carbon atom<sup>16,26</sup>, or a vacancy (here obtained in the  $V_0 \rightarrow \infty$  limit)<sup>26,32</sup>, as could be induced by proton irradiation<sup>33</sup>.

Fig. 2 shows the LDOS on a single site-like impurity, Eq. (19), for negative as well as for positive values of the impurity strength  $U_0 = V_0/a^2$ , where  $a$  is the lattice step, in the limit of weak scattering ( $|U_0| \ll 6t$ ). As anticipated, a bound state forms below the valence band if  $U_0 < 0$ , whereas a bound state forms above the conduction band for  $U_0 > 0$ .

From Eq. (19), a resonance is formed at an energy  $\omega_{res}$  between the two Van Hove singularities when

$$1 - V_0 \text{Re } G^0(\mathbf{x}, \mathbf{x}, \omega_{res}) = 0. \quad (21)$$

By inspection of the  $\omega$ -dependence of  $\text{Re } G^0(\omega)$  (Fig. 1), it follows that Eq. (21) is fulfilled for  $-1 < t/U_0 < \frac{1}{2}$ . Such a resonance is better resolved when the unperturbed LDOS  $\rho^0(\mathbf{x}, \mathbf{x}, \omega)$  is weak for  $\omega \approx \omega_{res}$ . This is indeed the case in the proximity of the Dirac points, where  $\rho^0(\mathbf{x}, \mathbf{x}, \omega) \rightarrow 0$  linearly as  $\omega \rightarrow 0$ . A special case is represented by the limit  $U_0 \rightarrow \infty$ , corresponding to a vacancy formation. In this case, the condition for a resonance is fulfilled at  $\omega \approx st$ , where however the LDOS is strongly depressed.

At exactly  $\omega = 0$ , *e.g.* when the chemical potential traverses the Dirac points, the resonance becomes a true bound state, since  $\rho^0(\mathbf{x}, \mathbf{x}, \omega) = 0$ . The value of the impurity potential  $U_0$  allowing a bound state at  $\omega = 0$  can

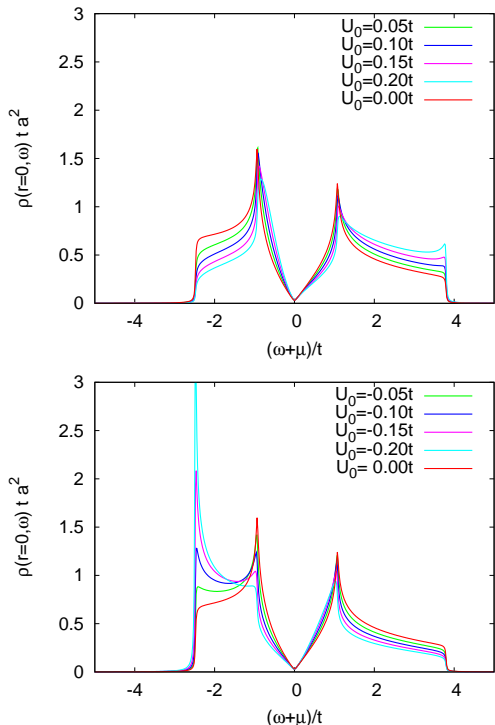


FIG. 2: (Color online) Local density of states  $\rho(\mathbf{x} = \mathbf{0}, \omega)$ , Eq. (19), on a site-like impurity located at  $\mathbf{x} = \mathbf{0}$ . Top panel shows the LDOS for  $U_0/t = -0.05, -0.10, -0.15, -0.20$ . Bottom panel shows the LDOS for  $U_0/t = 0.05, 0.10, 0.15, 0.20$ . In both panels, we also show the LDOS in the unperturbed case ( $U_0/t = 0$ ).

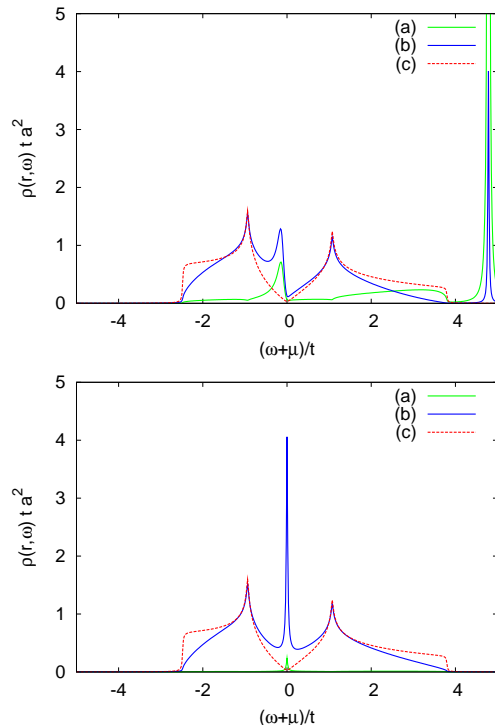


FIG. 4: (Color online) Showing the LDOS for a site-like impurity at  $\mathbf{x} = \mathbf{0}$  (a) on the impurity site, (b) on a nearest neighbor site, (c) on a generic lattice site in the unperturbed case. Top panel refers to low potential strength ( $U_0 = 1.1t$ ), while bottom panel refers to large potential strength ( $U_0 = 3.7t$ ).

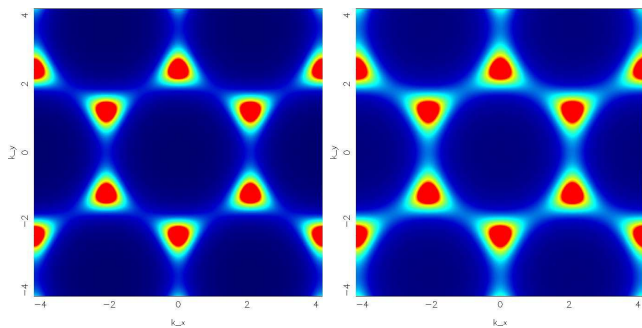


FIG. 3: (Color online) Contour plots of the LDOS in momentum space,  $\rho_\lambda(\mathbf{k}, \omega = 0)$ , Eq. (20), for the valence ( $\lambda = 1$ , left panel) and conduction band ( $\lambda = 2$ , right panel). Here, we are considering a site-like impurity with  $U_0 = 3.7t$ , thus giving rise to a bound state at  $\omega = 0$ .

be obtained within a semi-analytical approach (see Appendix B for details). This is based on an expansion of  $\text{Re}G^0(\mathbf{x}, \mathbf{x}, \omega = 0)$  in Eq. (21) at  $\mathbf{x} = \mathbf{0}$ . To the leading terms in the nearest neighbors, one finds that the condition for having a bound state at  $\omega = 0$  is

$$\frac{t}{U_0} \approx \phi(\mathbf{0})[s\phi(\mathbf{0}) + 2\phi(\delta_1)], \quad (22)$$

where  $\phi(\mathbf{x})$  is a gaussian pseudo-atomic wavefunction,  $s$  is the band asymmetry parameter, and  $\delta_1$  the position of a nearest neighbor to  $\mathbf{x} = \mathbf{0}$  (Appendix B). The first contribution to Eq. (22) is due to the band asymmetry ( $s \neq 0$ ), whereas the second contribution is related to the wavefunction width, and can be neglected for a sufficiently localized pseudo-atomic wavefunction. In the limit of symmetric bands ( $s = 0$ ) and localized wavefunctions, one recovers a bound state at exactly  $\omega = 0$  in the case of a vacancy ( $U_0 = \infty$ )<sup>7,11,15</sup>. From Eq. (22) one may conclude that a bound state is formed also in the case of a localized pseudoatomic wavefunction, provided one retains a nonzero band asymmetry ( $s \neq 0$ ), and that this takes place for a finite value of the impurity potential ( $U_0 < \infty$ ), in agreement with the findings of Ref. 7. Fig. 3 shows a contour plot of the LDOS in momentum space for an impurity potential generating a bound state at  $\omega = 0$ , for both the valence and conduction bands. In both cases, the largest contribution to  $\rho_\lambda(\mathbf{k}, \omega)$  comes from the wavevectors close to the Dirac points. Slight differences between the two bands are due to a nonzero asymmetry parameter  $s$ .

We end this subsection by considering the effect of a site-like impurity located at  $\mathbf{x} = \mathbf{0}$  on the LDOS at a neighboring site,  $\mathbf{y} = \delta_3$ , say. After the appropriate ana-

lytical continuation, Eq. (17) then yields

$$\rho(\mathbf{y}, \omega) \approx \frac{\text{Re} G^0(\mathbf{y}, \mathbf{x}, \omega) \text{Re} G^0(\mathbf{x}, \mathbf{y}, \omega)}{[\text{Re} G^0(\mathbf{x}, \mathbf{x}, \omega)]^2} \times V_0^{-1} \delta[1 - V_0 \text{Re} G^0(\mathbf{x}, \mathbf{x}, \omega)], \quad (23)$$

in the limit of vanishing unperturbed LDOS on the impurity,  $\rho^0(\mathbf{x}, \omega) \rightarrow 0$ . Therefore, while the condition for having a bound state on a neighboring site is the same as Eq. (21), the relative weight with respect to the impurity site is given by the prefactor in Eq. (23). Fig. 4 shows the LDOS on a neighboring site ( $\mathbf{y} = \delta_3$ ), when a site-like impurity is located at  $\mathbf{x} = \mathbf{0}$ . The LDOS corresponding to a bound state outside the band is larger on the impurity site than on the neighboring site. The opposite is true for the LDOS corresponding to the resonant state between the two Van Hove singularities, which is depressed on the impurity site than on the neighboring site. The same effect applies to the bound state between the two Van Hove singularities.

Such a behavior for resonant states in the energy range between the two Van Hove singularities is analogous to the one encountered in the  $d$ -density-wave (DDW) phase, which has been suggested as a viable description of the pseudogap phase in the high- $T_c$  cuprates<sup>34,35</sup>. In the DDW phase, the LDOS on an atomic site vanishes linearly as  $\omega \rightarrow 0$  for the pure system, and exhibits two Van Hove singularities, symmetric with respect to  $\mu = 0$ . It has been demonstrated<sup>36,37</sup> that a sufficiently strong localized impurity produces a resonance between the two Van Hove singularities. The LDOS associated to such a resonance in the DDW phase is larger on a nearest neighbor, than on the impurity site, in close analogy to what is here shown for an impurity in graphene, and in agreement with the findings of Ref. 14. In both cases, the quasiparticle bands are characterized by two inequivalent minima (the two Dirac points, in the case of graphene), so that scattering processes due to short-range impurities can be classified as intra-valley or inter-valley, depending on whether initial and final states lie close to the same or to different extrema, respectively. The peculiar behavior of the LDOS corresponding to resonant states at  $\omega \approx 0$  is related to inter-valley scattering, at variance with bound states outside the bandwidth. It is also relevant to note, in this context, that single-impurity scattering around a localized impurity has been suggested as a tool to distinguish between a DDW and a pseudogap phases, within the precursor pairing scenario<sup>38</sup>.

## B. Bond-like impurities

An impurity located between an  $A$  and  $B$  site only preserves the  $C_{2v}$  symmetry, and may be used to model an oxygen impurity between two carbon atoms<sup>16</sup>. This corresponds to three inequivalent positions in the real lattice, although local effects on each of them are related by rotations of multiples of  $2\pi/3$ . In the following, for

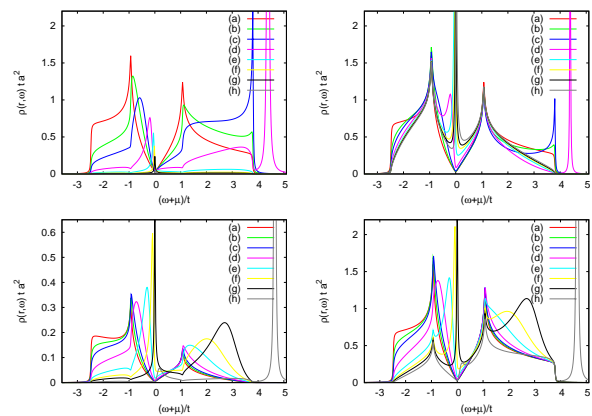


FIG. 5: (Color online) Local density of states for a site-like impurity (top row panels), and a bond-like impurity (bottom row panels). Left panel on top refers to the LDOS evaluated on the same position of a site-like impurity ( $\mathbf{r} = \mathbf{x} = \mathbf{0}$ ); right panel on top refers to the LDOS for a site-like impurity ( $\mathbf{x} = \mathbf{0}$ ), evaluated on a nearest neighbor lattice site ( $\mathbf{r} = \delta_1$ ). Left panel on bottom refers to the LDOS evaluated on the same position of a bond-like impurity ( $\mathbf{r} = \mathbf{x} = \delta_3/2$ ); right panel on bottom refers to the LDOS for a bond-like impurity ( $\mathbf{x} = \delta_3/2$ ), evaluated on a nearest neighbor lattice site ( $\mathbf{r} = \mathbf{0}$ ). The potential strengths are (a)  $U_0 = 0$ ; (b)  $U_0 = 0.05\tilde{U}_0$ ; (c)  $U_0 = 0.10\tilde{U}_0$ ; (d)  $U_0 = 0.25\tilde{U}_0$ ; (e)  $U_0 = 0.50\tilde{U}_0$ ; (f)  $U_0 = 0.75\tilde{U}_0$ ; (g)  $U_0 = \tilde{U}_0$ ; (h)  $U_0 = 2.00\tilde{U}_0$ , where  $\tilde{U}_0$  is the value of  $U_0$  yielding a bound state at  $\omega = 0$ .

definiteness, we shall therefore be concerned with a bond-like impurity located at  $\mathbf{x} = \delta_3/2$ .

With reference again to Eq. (19), one finds a markedly different  $\omega$ -dependence of  $G^0(\mathbf{x}, \mathbf{x}, \omega)$  at  $\mathbf{x} = \delta_3/2$  (Fig. 1), with respect to the site-like case ( $\mathbf{x} = \mathbf{0}$ ). Indeed, while  $\text{Im} G^0(\omega)$  is depressed with respect to the site-like case, as a consequence of the finite extent of the gaussian pseudoatomic wavefunctions,  $\text{Re} G^0(\omega)$  attains a finite value at  $\omega = \omega_T$  (Fig. 1). This implies the existence of bound states above the conduction band only for  $U_0 \gtrsim 8t$ , while bound states below the valence band still exists for any  $U_0 < 0$ . On the other hand, resonances between the two Van Hove singularities close to  $\omega = 0$  are possible for  $2 < U_0/t < 20$ , *i.e.* within a finite range of positive values of the impurity strength.

An expansion of  $\text{Re} G^0$  in Eq. (21), where now  $\mathbf{x} = \delta_3/2$ , leads to the estimate

$$\frac{t}{U_0} \approx (A_b + 2s) \phi^2(\delta_3/2) \quad (24)$$

for the impurity potential required to generate a bound state at  $\omega = 0$ , where  $A_b \simeq 0.67$  (Appendix B). As in the site-like case, one can recognize a term due to the asymmetry between the two bands ( $s \neq 0$ ).

Fig. 5 compares the LDOS for a site-like (top row panels) and a bond-like (bottom row panels) impurity, both evaluated on the same position as the impurity (left column panels) and on a nearest neighbor lattice site (right column panels), for several values of the po-



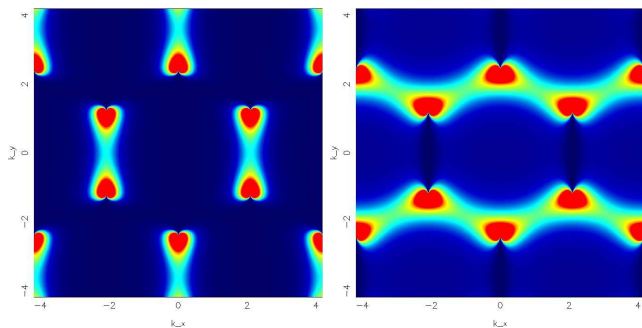


FIG. 6: (Color online) Contour plots of the LDOS in momentum space,  $\rho_\lambda(\mathbf{k}, \omega)$ , Eq. (20), for the valence ( $\lambda = 1$ , left panel) and conduction band ( $\lambda = 2$ , right panel). Here, we are considering a bond-like impurity with  $U_0 = 5.1t$ , thus giving rise to a bound state at  $\omega = 0$ .

tential strength. One finds quite a different behavior in the two cases. As  $U_0$  increases towards  $\tilde{U}_0$ , *i.e.* the value of the impurity strength giving rise to a bound state at  $\omega = 0$ , the LDOS on the impurity site, and the weight of the Van Hove singularities, decreases, as expected. On the other hand, the bound state at  $\omega = 0$  becomes sharper and more pronounced in the bond-like case, whereas it becomes suppressed in the site-like case. Another remarkable difference is the presence, in the bond-like case, of a wide resonant state in the conduction band for  $4t \lesssim U_0 \lesssim 8t$ , which is completely absent in the site-like case. This can be traced back to the different  $\omega$ -dependence of  $\text{Re}G^0$  in Eq. (21) in the two cases. Fig. 5 also compares the LDOS for the site-like and bond-like cases, but now evaluated on a nearest neighbor lattice site to the impurity position. Again, the Van Hove singularities become smoother, as  $U_0$  increases towards  $\tilde{U}_0$ . The suppression of the singularities due to an increase in the potential strength is enhanced in the bond-like case, than in the site-like case.

Finally, Fig. 6 shows the LDOS in momentum space, Eq. (20), in the case of a bond-like impurity at  $\mathbf{x} = \delta_3/2$ , for the valence and conduction bands. Fig. 6 refers to a potential strength of  $U_0 = 5.1t$ , thus giving rise to a bound state at  $\omega = 0$ . Similar pictures, but rotated at multiples of  $2\pi/3$ , would be obtained in the other, inequivalent, bond-like positions. As in the site-like case, Fig. 3, one finds that the points in  $\mathbf{k}$ -space providing the largest contribution to  $\rho_\lambda(\mathbf{k}, \omega)$  are those closer to the Dirac points, but now with a reduced symmetry. In particular,  $\rho_\lambda(\mathbf{k}, \omega)$  is not invariant with respect to transformations of the  $C_{6v}$  point group because of the squared modulus of the pseudoatomic wavefunctions in Eq. (20).

### C. Hollow-like impurities

The last case considered here corresponds to having a single impurity located at the center of an hexagon

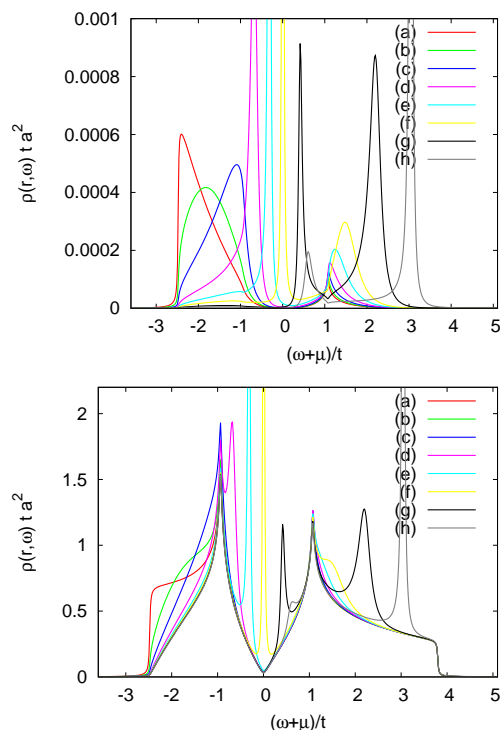


FIG. 7: (Color online) Local density of states for a hollow-like impurity ( $\mathbf{x} = -\delta_3$ ) on the same site as the impurity (top panel,  $\mathbf{r} = \mathbf{x}$ ), and on a nearest neighbor lattice site (bottom panel,  $\mathbf{r} = \mathbf{0}$ ). The potential strengths are (a)  $U_0 = 0$ ; (b)  $U_0 = 0.10\tilde{U}_0$ ; (c)  $U_0 = 0.25\tilde{U}_0$ ; (d)  $U_0 = 0.50\tilde{U}_0$ ; (e)  $U_0 = 0.75\tilde{U}_0$ ; (f)  $U_0 = \tilde{U}_0$ ; (g)  $U_0 = 1.50\tilde{U}_0$ ; (h)  $U_0 = 2.00\tilde{U}_0$ , where  $\tilde{U}_0$  is the value of  $U_0$  yielding a bound state at  $\omega = 0$ .

plaquette,  $\mathbf{x} = -\delta_3$ , say. This is the highest symmetry position in the carbon honeycomb lattice, and indeed the point symmetry  $D_{6h}$  is preserved. Inspection of Fig. 1 for the  $\omega$ -dependence of  $\text{Re}G^0(\omega)$  and  $\rho^0(\omega)$  shows that the unperturbed LDOS is severely depressed (some three orders of magnitude lower) than the LDOS in the site-like case. Moreover, as a consequence of the overall behavior of  $\text{Re}G^0(\omega)$ , one has a bound state below the valence band for all negative values of  $U_0$ , whereas one has a bound state above the conduction band for relatively large positive values of the impurity strength,  $U_0 \gtrsim 10^4 t$ . On the other hand, the relatively low value of  $\rho^0(\omega)$  allows the formation of well-resolved resonant states close to  $\omega = 0$ , for  $1.5 \cdot 10^3 t \lesssim U_0 \lesssim 1.1 \cdot 10^4 t$ . Expanding  $\text{Re}G^0$  in Eq. (21), where now  $\mathbf{x} = -\delta_3$ , yields in this case the estimate

$$\frac{t}{U_0} \approx (A_h + 2B_h s) \phi^2(\delta_3) \quad (25)$$

for the impurity potential required to generate a bound state at  $\omega = 0$ , where  $A_h \simeq 2.35$  and  $B_h = 3$  (Appendix B). As in the previous cases, the main term persists also in the limit of perfect band symmetry ( $s = 0$ ).

Fig. 7 shows the LDOS for a hollow-like impurity, both on top of the impurity site, and on an adjacent lattice

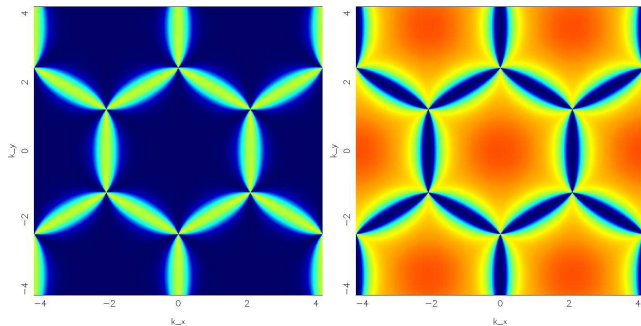


FIG. 8: (Color online) Contour plots of the LDOS in momentum space,  $\rho_\lambda(\mathbf{k}, \omega)$ , Eq. (20), for the valence ( $\lambda = 1$ , left panel) and conduction band ( $\lambda = 2$ , right panel). Here, we are considering a hollow-like impurity with  $U_0 = 3.8 \cdot 10^4 t$ , thus giving rise to a bound state at  $\omega = 0$ .

site, for several potential strengths. At variance from the previous two cases, it is apparent that resonant states are sharper in the nearest neighbor site, than on top of the impurity position. Analogously to the bond-like case, there are resonant states developing in the high conduction band, which are however better defined.

Fig. 8 shows the LDOS in momentum space, for a hollow-like impurity giving rise to a bound state at  $\omega = 0$ , Eq. (25). At variance with the previous cases, one may notice that the  $\mathbf{k}$ -states contributing most importantly to  $\rho_\lambda(\mathbf{k}, \omega)$  are the same as those involved in building up the unperturbed LDOS. Indeed, in the conduction band ( $\omega > 0$ ), the largest contributions to  $\rho^0(-\delta_3, -\delta_3, \omega)$  come from the Van Hove singularities and the centers of the sides of the first Brillouin zone. Similarly, in the valence band ( $\omega < 0$ ), the largest contributions to  $\rho^0(-\delta_3, -\delta_3, \omega)$  come from the band bottom, *i.e.* from  $\mathbf{k}$ -points close to the  $\Gamma$  point. This can be ultimately be traced back to the extended width of the gaussian pseudoatomic wavefunction here employed.

#### IV. MANY IMPURITIES

While single impurity effects are in principle observable through STM measurements<sup>12,17,18</sup>, real samples usually contain a sizeable amount of impurities, which are responsible of sensible modifications of both thermodynamic and transport properties. Therefore, we will here exploit the results of Sec. III for a single impurity, to study the effect of  $N_{imp}$  impurities on a graphene monolayer. We will assume that (i) the position of all impurities differ by a vector of the direct lattice; in other words, there is a preferential kind of impurity location, *i.e.* all impurities are either site-like, bond-like, or hollow-like, according to the classification given in the Sec. III; (ii) impurities are independent, *i.e.* the average distance between two impurities is larger than the quasiparticle coherence length, so that interference ef-

fects can be neglected; (iii) their number is sufficiently large ( $N_{imp} \gg 1$ ), so that their effect is appreciable on bulk properties in the thermodynamic limit, but the impurities are sufficiently diluted ( $n_{imp} = N_{imp}/N \ll 1$ ). In these limits, while a standard averaging procedure over the position configurations of the impurities restores the translational invariance of the Green's function,

$$\mathcal{G}_{\lambda\lambda'}^{imp}(\mathbf{k}, \mathbf{k}', i\omega_n) = \delta_{\mathbf{k}\mathbf{k}'} \mathcal{G}_{\lambda\lambda'}^{imp}(\mathbf{k}, i\omega_n), \quad (26)$$

the eigenstates of the pure Hamiltonian are expected to acquire a finite lifetime induced by disorder. This can be formally achieved by relating  $\mathcal{G}^{imp}(\mathbf{k}, i\omega_n)$ , now a matrix with respect to the band indices, to the single-impurity Green's function  $\mathcal{G}^0(\mathbf{k}, i\omega_n)$  discussed in Sec. III through a Dyson's equation analogous to Eq. (13), but now involving the proper self energy matrix<sup>27</sup>  $\Sigma(\mathbf{k}, i\omega_n)$

$$\mathcal{G}^{imp}(\mathbf{k}, i\omega_n) = \mathcal{G}^0(\mathbf{k}, i\omega_n) + \mathcal{G}^0(\mathbf{k}, i\omega_n) \Sigma(\mathbf{k}, i\omega_n) \mathcal{G}^{imp}(\mathbf{k}, i\omega_n). \quad (27)$$

Within the full Born approximation (FBA)<sup>27</sup>, which is valid in the limit of small impurity concentration,  $n_{imp}^2 \ll n_{imp}$ , one finds

$$\Sigma_{\lambda\lambda'}(\mathbf{k}, i\omega_n) = n_{imp} \frac{V_0 \tilde{\psi}_{\mathbf{k}\lambda}^*(\mathbf{x}) \tilde{\psi}_{\mathbf{k}\lambda'}(\mathbf{x})}{1 - \frac{V_0}{N} \sum_{\mathbf{q}\lambda''} |\tilde{\psi}_{\mathbf{k}\lambda''}(\mathbf{x})|^2 \mathcal{G}_{\lambda''}^0(\mathbf{q}, i\omega_n)}, \quad (28)$$

where we are assuming that all impurities occupy equivalent lattice positions. Comparing Eq. (28) with Eqs. (15) and (16), it is possible to relate the proper self-energy within the FBA to the  $T$ -matrix for the same kind of impurity, through

$$\Sigma_{\lambda\lambda'} = N_{imp} T_{\lambda\lambda'}(\mathbf{x}; \mathbf{k}, \mathbf{k}', i\omega_n). \quad (29)$$

Eq. (29) therefore enables us to generalize most of the results derived in Sec. III to the case of many impurities, all located within a preferential class of lattice positions.

##### A. LDOS

We begin by discussing the effect of many impurities on the local density of states in reciprocal space. This can be obtained by inverting Eq. (27) for  $\mathcal{G}^{imp}(\mathbf{k}, i\omega_n)$  and then performing the usual analytical continuation. Most properties can be derived by describing the behavior of the analytically-continued proper self-energy, which in all of the three cases of interest can be written as

$$\Sigma(\mathbf{k}, \omega) = n_{imp} \frac{V_0 W(\mathbf{k})}{1 - V_0 G^0(\mathbf{x}, \mathbf{x}, \omega)}, \quad (30)$$

where  $\mathbf{x} = \mathbf{0}$ ,  $\delta_3/2$ , or  $-\delta_3$  in the site-like, bond-like, or hollow-like case, respectively, and  $W(\mathbf{k})$  is a matrix form



factor explicitly given by

$$W_{\lambda\lambda'}^{(s)}(\mathbf{k}) = \frac{1}{2}[\check{\psi}_{\mathbf{k}\lambda}^*(\mathbf{0})\check{\psi}_{\mathbf{k}\lambda'}(\mathbf{0}) + \check{\psi}_{\mathbf{k}\lambda}^*(\delta_3)\check{\psi}_{\mathbf{k}\lambda'}(\delta_3)] \quad (31a)$$

$$W_{\lambda\lambda'}^{(b)}(\mathbf{k}) = \frac{1}{3} \sum_{\ell=1}^3 \check{\psi}_{\mathbf{k}\lambda}^*(\delta_\ell/2)\check{\psi}_{\mathbf{k}\lambda'}(\delta_\ell/2) \quad (31b)$$

$$W_{\lambda\lambda'}^{(h)}(\mathbf{k}) = \check{\psi}_{\mathbf{k}\lambda}^*(-\delta_3)\check{\psi}_{\mathbf{k}\lambda'}(-\delta_3) \quad (31c)$$

in the site-like, bond-like, and hollow-like cases, respectively. We are here assuming that the impurities are equally distributed among the  $A$  and  $B$  sites, in the site-like case, and among the three classes of  $\sigma$  bonds, in the bond-like case.

Both in the site-like and in the bond-like cases, direct inspection of the solution of Eq. (27) shows that  $G^{imp}(\mathbf{k}, \omega)$  is nearly diagonal in the diluted limit ( $n_{imp}^2 \ll n_{imp}$ ). Therefore, an eigenstate of the unperturbed Hamiltonian labelled by wavevector  $\mathbf{k}$  and band index  $\lambda$  acquires a finite lifetime  $\tau_{\mathbf{k}\lambda}$ , which *e.g.* in the site-like case and in the limit of low LDOS is given by

$$\tau_{\mathbf{k}\lambda}^{-1} \approx \pi n_{imp} V_0^2 W_{\lambda\lambda}(\mathbf{k}) \rho(\mathbf{0}, \omega = \xi_{\mathbf{k}\lambda}), \quad (32)$$

where  $\rho(\mathbf{x}, \omega)$  is the LDOS with a single impurity, Eq. (19).

For impurity potentials close to the condition for a well-defined resonance at  $\omega \approx 0$  in the single-impurity case, Eq. (21), in the dilute limit, one gets for the LDOS in reciprocal space close to a Dirac point

$$\rho_\lambda(\mathbf{k}, \omega) \approx \frac{A_{\mathbf{k}\lambda}}{[\omega - \xi_{\mathbf{k}\lambda} + B_{\mathbf{k}\lambda}(\omega - \xi_{\mathbf{k}\bar{\lambda}})]^2 + \pi^2 A_{\mathbf{k}\lambda}^2}, \quad (33)$$

where  $\bar{\lambda} = 2$  when  $\lambda = 1$ , and  $\bar{\lambda} = 1$  when  $\lambda = 2$ , and

$$A_{\mathbf{k}\lambda} = n_{imp} V_0^2 W_{\lambda\lambda}(\mathbf{k}) \rho_\lambda(\mathbf{0}, \omega) \times \left[ 1 - \frac{W_{12}(\mathbf{k})W_{21}(\mathbf{k})}{W_{11}(\mathbf{k})W_{22}(\mathbf{k})} \right], \quad (34a)$$

$$B_{\mathbf{k}\lambda} = \frac{W_{12}(\mathbf{k})W_{21}(\mathbf{k})}{W_{\lambda\lambda}^2(\mathbf{k})}. \quad (34b)$$

The behavior of the LDOS in reciprocal space is therefore quite different from the unperturbed case, which would be characterized by a Dirac delta peaked along closed contours around the Dirac points.

The case in which all impurities are located in a hollow-like position, Eq. (31c), is quite different from the previous two cases, Eqs. (31a) and (31b). This is due to the fact that the form factors  $W(\mathbf{k})$  defined in Eq. (31c) fulfill the additional identity  $W_{11}(\mathbf{k})W_{22}(\mathbf{k}) - W_{12}(\mathbf{k})W_{21}(\mathbf{k}) = 0$ .

While the Born approximation holds for low impurity concentration,  $n_{imp}^2 \ll n_{imp}$ , one has to distinguish two regimes. For moderately large impurity concentrations,  $n_{imp} \gg t |\text{Im} G^0(-\delta_3, \omega_{res})|$ , for an impurity potential close to what would be a resonance in the single-impurity

case, one finds a nearly diagonal Green's function, whose nonzero matrix elements are given by

$$G_{\lambda\lambda}^{imp} \approx \left[ \omega - \xi_{\lambda\mathbf{k}} + \frac{W_{\lambda\lambda}(\mathbf{k})}{W_{\lambda\bar{\lambda}}(\mathbf{k})} (\omega - \xi_{\bar{\lambda}\mathbf{k}}) + \frac{i W_{\lambda\lambda}(\mathbf{k})}{\pi W_{\lambda\bar{\lambda}}^2(\mathbf{k})} \frac{(\omega - \xi_{\bar{\lambda}\mathbf{k}})^2}{n_{imp} V_0^2 \rho(-\delta_3, \omega)} \right]^{-1}. \quad (35)$$

In the same limit, for an impurity potential giving rise to a resonance at exactly  $\omega = 0$ , the situation is even more dramatic, since

$$G_{\lambda\lambda}^{imp} \approx \left[ - \left( \xi_{\lambda\mathbf{k}} + \frac{W_{\lambda\lambda}(\mathbf{k})}{W_{\lambda\bar{\lambda}}(\mathbf{k})} \xi_{\bar{\lambda}\mathbf{k}} \right) + i\eta \right]^{-1}, \quad (36)$$

where  $\eta$  is a positive infinitesimal. On the other hand, for  $n_{imp} \ll t |\text{Im} G^0(-\delta_3, \omega_{res})|$ , one finds

$$G_{\lambda\lambda}^{imp} \approx [\omega - \xi_{\lambda\mathbf{k}} + i\pi n_{imp} V_0^2 \rho(-\delta_3, \omega) W_{\lambda\lambda}(\mathbf{k})]^{-1}. \quad (37)$$

The different behavior with respect to the previous two cases follows from the fact that in the hollow-like case the Born approximation performs an average with respect to impurity positions all of the same kind, at variance, *e.g.* with the site-like case, where impurities can be added either in the  $A$  or in the  $B$  sublattices. This is likely to produce an additional dephasing among contributions arising from inequivalent lattice positions in the site-like or bond-like cases, with respect to the hollow-like case, thereby resulting in an increasing inverse lifetime with increasing impurity concentration, although only in the moderately low impurity concentration, Eq. (35). One however recovers the physically expected behavior at low impurity concentrations, *i.e.* a vanishing inverse lifetime with increasing impurity concentration, Eq. (37).

## B. Conductivity

We end this section by considering the effect of many, short-range impurities on the conductivity. As described above, we are mainly concerned with the case in which all impurities are located in the same class of lattice positions, and we will here focus on the site-like case, even though, as described in Sec. IV A, the analysis presented here is actually more general, as it qualitatively applies also to the bond-like case, at least for  $\mu$  between the two Van Hove singularities. Again, we will assume the dilute regime,  $n_{imp}^2 \ll n_{imp}$ , so that the full Born approximation holds.

Within linear response theory, the conductivity  $\sigma$  is related to the current-current correlation function through a Kubo formula

$$\sigma_{lm}(\mu, T; \omega) = \frac{ie^2 n}{m\omega} \delta_{lm} + \frac{i}{\hbar\omega N A_{cell}} \tilde{\Pi}_{lm}^R(0, 0, \omega), \quad (38)$$

where  $n$  is the electron density,  $\omega$  is the frequency of the external electric field,  $A_{cell}$  is the area of a primitive cell,

and  $\tilde{\Pi}_{lm}^R(\mathbf{k}, \mathbf{q}, \omega)$  is the  $(l, m)$  component of the Fourier transform of the retarded current-current correlation tensor. We are mainly interested in the dissipative part of the conductivity tensor, *i.e.* its real part. For the longitudinal part  $\sigma = \text{Re } \sigma_{xx}$ , one has

$$\sigma(\mu, T; \omega) = -\frac{1}{\hbar\omega N A_{\text{cell}}} \text{Im } \tilde{\Pi}_{xx}^R(0, 0, \omega), \quad (39)$$

where  $\tilde{\Pi}_{lm}^R$  is the retarded version of

$$\tilde{\Pi}_{lm}(\mathbf{k}, \mathbf{q}, \tau) = -\langle T_\tau [\tilde{J}_l^\nabla(\mathbf{k}, \tau) \tilde{J}_m^\nabla(\mathbf{q}, 0)] \rangle, \quad (40)$$

and  $\tilde{J}_l^\nabla(\mathbf{k}, \tau)$  denote the Fourier transform of the paramagnetic component of the current density vector, at the imaginary time  $\tau$ . Expanding  $\tilde{J}_l^\nabla(\mathbf{k}, \tau)$  in terms of the eigenstates of the unperturbed Hamiltonian, and making use of the results of Appendix C, one finds

$$\tilde{\Pi}_{xx}(0, 0, \tau) = e^2 \frac{t^2 a^2}{\hbar^2} \sum_{\substack{\mathbf{k}\mathbf{k}' \\ \lambda\lambda'\eta\eta'}} h_{x,\lambda\eta}(\mathbf{k}) h_{x,\lambda'\eta'}(\mathbf{k}') \langle T_\tau [c_{\mathbf{k}\lambda}^\dagger(\tau^+) c_{\mathbf{k}\eta}(\tau) c_{\mathbf{k}'\lambda'}^\dagger(0^+) c_{\mathbf{k}'\eta'}(0)] \rangle, \quad (41)$$

where the matrix elements  $\mathbf{h}_{m,\lambda\eta}(\mathbf{x})$  are defined in Appendix C. One is now in the position to make use of Wick's theorem. We further make the approximation to treat the one-body Green's functions within the FBA, and perform the required analytical continuation, to obtain

$$\begin{aligned} \tilde{\Pi}_{xx}^R(0, 0, \omega) &= 2e^2 \frac{t^2 a^2}{\hbar^2} \sum_{\substack{\mathbf{k} \\ \lambda\lambda'\eta\eta'}} h_{x,\lambda\eta}(\mathbf{k}) h_{x,\lambda'\eta'}(\mathbf{k}) \int_{-\infty}^{\infty} \frac{d\zeta}{2\pi i \hbar} \left\{ [n_F(\zeta + \omega) - n_F(\zeta)] G_{\lambda\eta'}^{imp*}(\mathbf{k}, \zeta) G_{\eta\lambda'}^{imp}(\mathbf{k}, \zeta + \omega) \right. \\ &\quad \left. + n_F(\zeta) G_{\eta'\lambda}^{imp}(\mathbf{k}, \zeta) G_{\eta\lambda'}^{imp}(\mathbf{k}, \zeta + \omega) - n_F(\zeta + \omega) G_{\lambda\eta'}^{imp*}(\mathbf{k}, \zeta) G_{\lambda'\eta}^{imp*}(\mathbf{k}, \zeta + \omega) \right\}, \end{aligned} \quad (42)$$

where  $n_F(\omega)$  is the Fermi function, and the factor of 2 takes into account for spin degeneracy.

We next make a further approximation, *i.e.* we assume that the impurity Green's functions are diagonal in the band index,  $G_{\lambda\lambda'}^{imp}(\mathbf{k}, \omega) \approx \delta_{\lambda\lambda'} G_{\lambda\lambda}^{imp}(\mathbf{k}, \omega)$ . Such an approximation is justified in the dilute limit, and amounts to treat the effect of disorder as a perturbation to the pure case, whose main effect is that of adding a finite lifetime to the eigenstates of the unperturbed Hamiltonian.

In the static limit ( $\omega \rightarrow 0$ ) and at  $T = 0$ , Eq. (39) yields the conductivity as a function of the chemical potential, which can be decomposed in an inter- and intra-band contribution,  $\sigma_{\text{DC}}(\mu) = \sigma_{\text{inter}}(\mu) + \sigma_{\text{intra}}(\mu)$ , given by

$$\begin{aligned} \frac{\sigma_{\text{inter}}(\mu)}{\sigma_0} &= -\frac{1}{\tau_0^2} \frac{1}{N} \sum_{\mathbf{k}} h_{x,12}(\mathbf{k}) h_{x,21}(\mathbf{k}) \\ &\quad \times \text{Im } G_{11}^{imp}(\mathbf{k}, 0) \text{Im } G_{22}^{imp}(\mathbf{k}, 0) \end{aligned} \quad (43a)$$

$$\frac{\sigma_{\text{intra}}(\mu)}{\sigma_0} = -\frac{1}{\tau_0^2} \frac{1}{N} \sum_{\mathbf{k}, \alpha=1,2} [h_{x,\alpha\alpha}(\mathbf{k}) \text{Im } G_{\alpha\alpha}^{imp}(\mathbf{k}, 0)]^2 \quad (43b)$$

where  $\sigma_0 = \pi e^2 / (2h)$  is proportional to the quantum of conductivity, and  $\tau_0^{-2} = 16t^2 / (3\sqrt{3}\pi\hbar^2)$ . One may expect that the interband contribution, Eq. (43a), only

becomes comparable with the intraband contribution, Eq. (43b), when  $\mu \approx 0$ , *i.e.* when the valence and conduction bands overlap, owing to the disorder-induced energy spread. Away from neutrality ( $\mu = 0$ ), and for a given impurity potential strength  $U_0$ , an increase of the Fermi surface width produces an increase of the conductivity. Such an increase is however rather slow, close to the energy values where the LDOS with a single impurity is maximum, where the backscattering due to the impurities is more effective. Such a sublinear increase of  $\sigma_{\text{DC}}$  as a function of the carrier concentration  $n$  occurs for values of  $U_0$  giving rise to resonant states close to  $\mu = 0$  and does not depend on the value of  $n_{\text{imp}}$ . Such a behavior is numerically confirmed in Fig. 9, for various values of  $n_{\text{imp}}$  and  $U_0$ , and is in good qualitative agreement with the experimental results<sup>22</sup>. The asymmetry between the particle ( $n > 0$ ) and hole ( $n < 0$ ) regimes is partly due to the band asymmetry ( $s \neq 0$ ), but is mainly due to the effect of impurities, which is different depending on the sign of  $\mu$ . Both in the valence and conduction bands, however, one observes the occurrence of a maximum and then a decrease of  $\sigma_{\text{DC}}$  when  $\mu$  attains the value corresponding to a Van Hove singularity, where the Fermi surface is maximally extended and traverses an electronic topological transition. A comparison between the two panels in Fig. 9 shows that the nonmonotonic behavior of  $\sigma_{\text{DC}}$  is generic for all impurity concentrations, but

rather depends on the impurity potential  $U_0$ . The similarity between Fig. 9 and the concentration dependence of the conductivity measured in suspended graphene after annealing surmises that scattering due to short range impurities is relevant to determine the transport properties of these graphene samples<sup>23,24,39</sup>.

## V. CONCLUSIONS

We have analyzed the effects of a single, localized impurity on the local electronic properties of a graphene monolayer. Specifically, we have considered an isolated impurity located on high-symmetry positions of the honeycomb lattice, such as the site-like, bond-like, and hollow-like positions. While the electronic properties of the pure system have been treated within the tight-binding approximation, but allowing for asymmetry between valence and conduction bands, the effect of the impurity has been modelled through a gaussian pseudoatomic wavefunction, even though more general functional forms have been taken into account. Moreover, the tight binding scheme employed in this work does not suffer from the ‘cone approximation’<sup>11,15</sup>, thereby enabling

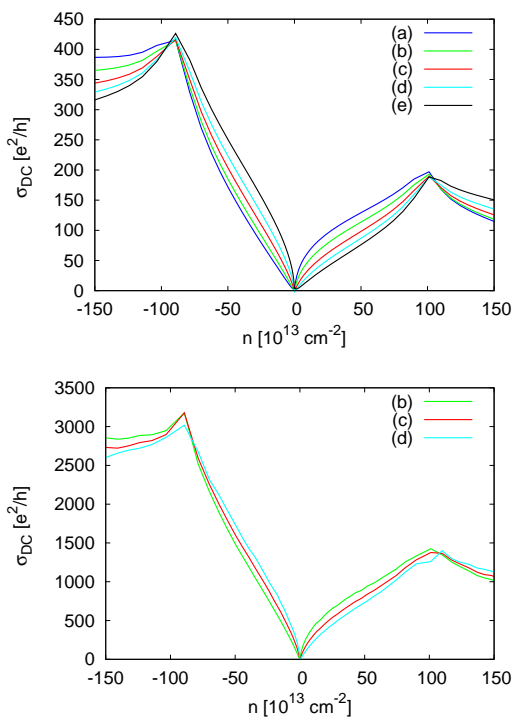


FIG. 9: (Color online) Conductivity  $\sigma_{DC}$  as a function of the carrier concentration  $n$  in graphene, in the presence of many site-like impurities. The upper panel refers to a value  $n_{imp} = 10^{-2}$  of the impurity concentration, while the lower panel is characterized by  $n_{imp} = 10^{-3}$ . The impurity potentials under consideration are (a)  $U_0 = 0.35\tilde{U}_0$ , (b)  $U_0 = 0.50\tilde{U}_0$ , (c)  $U_0 = \tilde{U}_0$ , (d)  $U_0 = 10.00\tilde{U}_0$ , (e)  $U_0 = -\tilde{U}_0$ , where  $\tilde{U}_0$  is the potential strength giving rise to a bound state at  $\omega = 0$ .

one to treat both low and high energies within the band with the same degree of accuracy.

We have evaluated the local density of states as a function of energy on the impurity site and on its nearest neighbor locations, and as a function of wavevector in reciprocal space, close to a resonance. The latter may be of relevance to interpret FTSTS measurements around an impurity. In particular, it has been shown that the main contributions to the impurity-induced modification of the LDOS come from wavevectors close to the Dirac point, in the site-like and bond-like cases, while the same states are involved in determining the LDOS both in the unperturbed case and in the case of a hollow-like impurity. Moreover, it has been suggested that FTSTS spectra can be used to distinguish between different types of impurities, in particular as far as the impurity potential range is concerned<sup>9</sup>.

We have determined semi-analytically the condition on the impurity strength for having a bound state at  $\omega = 0$  in the three cases of interest. In particular, in the site-like case, it is shown that the weight associated with a bound state between the two Van Hove singularities is larger for the LDOS on a neighboring site, than on the impurity site itself. Such a behavior is analogous to the one predicted for the  $d$ -density-wave state of high- $T_c$  superconductors, and can be attributed to the different contributions coming from intra- and inter-valley impurity scattering.

Our results for the single-impurity case have been exploited to discuss the effect of distributed impurities, all located in a preferential class of lattice sites. Such a generalization has been derived within the full Born approximation, and applies to the dilute limit. In particular, we have estimated the quasiparticle lifetime associated to a finite impurity concentration, and the behavior of the LDOS in reciprocal space. Within linear response theory, we have also evaluated the static conductivity. One can again distinguish an intra- and an inter-band contribution, the latter being sizeable only close to zero carrier concentration, *i.e.* when the two bands appreciably overlap. Moving away from neutrality, one recovers a nonmonotonic dependence on the carrier concentration, characterized by a sublinear increase close to  $\mu = 0$ , as is observed experimentally in suspended graphene samples after annealing. Such a feature is generic, in the sense that it applies to all impurity concentrations under study, and rather depends on the impurity strength.

## Acknowledgments

The authors are indebted with Professor N. H. March for valuable discussions over the general area embraced by the present work.

## APPENDIX A: DYSON EQUATION FOR SEPARABLE IMPURITY POTENTIAL

Here, we briefly derive Dyson's equation, Eq. (14), in the case of a separable impurity potential, Eq. (3). Inserting our Ansatz for the potential, Eq. (3), into Eq. (13), and iterating, one may express the Green's func-

tion  $\mathcal{G}_{\lambda\lambda'}(\mathbf{k}, \mathbf{k}', i\omega_n)$  as a series<sup>27</sup>,

$$\mathcal{G}_{\lambda\lambda'}(\mathbf{k}, \mathbf{k}', i\omega_n) = \sum_{\ell=0}^{\infty} \mathcal{G}_{\lambda\lambda'}^{(\ell)}(\mathbf{k}, \mathbf{k}', i\omega_n), \quad (\text{A1})$$

whose first and successive terms are given iteratively by

$$\mathcal{G}_{\lambda\lambda'}^{(0)}(\mathbf{k}, \mathbf{k}', i\omega_n) = \delta_{\lambda\lambda'} \delta_{\mathbf{k}\mathbf{k}'} \mathcal{G}_{\lambda}^{(0)}(\mathbf{k}, i\omega_n) \quad (\text{A2a})$$

$$\mathcal{G}_{\lambda\lambda'}^{(\ell)}(\mathbf{k}, \mathbf{k}', i\omega_n) = \mathcal{G}_{\lambda\lambda'}^{(\ell-1)}(\mathbf{k}, \mathbf{k}', i\omega_n) + V_0 \sum_{\mathbf{q}\lambda''} \mathcal{G}_{\lambda\lambda''}^{(\ell-1)}(\mathbf{k}, \mathbf{q}, i\omega_n) \psi_{\mathbf{q}\lambda''}^*(\mathbf{x}) \psi_{\mathbf{k}'\lambda'}(\mathbf{x}) \mathcal{G}_{\lambda'}^{(0)}(\mathbf{k}', i\omega_n). \quad (\text{A2b})$$

This leads to the series

$$\begin{aligned} \mathcal{G}_{\lambda\lambda'}(\mathbf{k}, \mathbf{k}', i\omega_n) &= \delta_{\lambda\lambda'} \delta_{\mathbf{k}\mathbf{k}'} \mathcal{G}_{\lambda}^{(0)}(\mathbf{k}, i\omega_n) \\ &+ V_0 \mathcal{G}_{\lambda}^{(0)}(\mathbf{k}, i\omega_n) \psi_{\mathbf{k}\lambda}^*(\mathbf{x}) \psi_{\mathbf{k}'\lambda'}(\mathbf{x}) \mathcal{G}_{\lambda'}^{(0)}(\mathbf{k}', i\omega_n) \\ &+ V_0 \mathcal{G}_{\lambda}^{(0)}(\mathbf{k}, i\omega_n) \psi_{\mathbf{k}\lambda}^*(\mathbf{x}) \left( \sum_{\mathbf{q}\lambda''} V_0 \psi_{\mathbf{q}\lambda''}^*(\mathbf{x}) \mathcal{G}_{\lambda''}^{(0)}(\mathbf{q}, i\omega_n) \psi_{\mathbf{q}\lambda''}(\mathbf{x}) \right) \psi_{\mathbf{k}'\lambda'}(\mathbf{x}) \mathcal{G}_{\lambda'}^{(0)}(\mathbf{k}', i\omega_n) \\ &+ \dots \\ &+ V_0 \mathcal{G}_{\lambda}^{(0)}(\mathbf{k}, i\omega_n) \psi_{\mathbf{k}\lambda}^*(\mathbf{x}) \left( \sum_{\mathbf{q}\lambda''} V_0 \psi_{\mathbf{q}\lambda''}^*(\mathbf{x}) \mathcal{G}_{\lambda''}^{(0)}(\mathbf{q}, i\omega_n) \psi_{\mathbf{q}\lambda''}(\mathbf{x}) \right)^{\ell-1} \psi_{\mathbf{k}'\lambda'}(\mathbf{x}) \mathcal{G}_{\lambda'}^{(0)}(\mathbf{k}', i\omega_n) \\ &+ \dots, \end{aligned} \quad (\text{A3})$$

which is recognized as a geometric series, whose sum can be cast in the form of Eq. (14).

## APPENDIX B: EXPANSION OF THE BLOCH WAVEFUNCTIONS IN THE SUBLATTICE REPRESENTATION

At the origin of the  $A$  sublattice,  $\mathbf{r} = \mathbf{0}$  say, the Bloch wavefunctions can be expanded as

$$\psi_{\mathbf{k}A}(\mathbf{0}) = \phi_A^{(0)} + \phi_A^{(1)} \beta_{\mathbf{k}}^{(1)} + \phi_A^{(2)} \beta_{\mathbf{k}}^{(2)} + \dots \quad (\text{B1a})$$

$$\psi_{\mathbf{k}B}(\mathbf{0}) = \phi_B^{(1)} \gamma_{\mathbf{k}}^{(1)} + \phi_B^{(2)} \gamma_{\mathbf{k}}^{(2)} + \dots, \quad (\text{B1b})$$

where  $\beta_{\mathbf{k}}^{(n)}$  and  $\gamma_{\mathbf{k}}^{(n)}$  are basis functions of the trivial irreducible representation of the point group  $D_{6h}$  and  $D_{3h}$ , respectively. In particular, one finds  $\gamma_{\mathbf{k}}^{(1)} \equiv \gamma_{\mathbf{k}}$ , Eq. (5), while  $\beta_{\mathbf{k}}^{(1)} \equiv \beta_{\mathbf{k}}$ , with

$$\beta_{\mathbf{k}} = \sum_j' e^{i\mathbf{k}\cdot\mathbf{R}_j}, \quad (\text{B2})$$

where the prime restricts the summation to all next nearest neighbors in the direct lattice, *i.e.*  $|\mathbf{R}_j| = \sqrt{3}a$ .

Because of the rapid decrease of the gaussian pseudoatomic wavefunction, Eq. (6), one may safely truncate the expansions Eqs. (B1) to the first terms, thereby ob-

taining

$$\psi_{\mathbf{k}A}(\mathbf{0}) \approx \frac{1}{\sqrt{N}} \phi(\mathbf{0}), \quad (\text{B3a})$$

$$\psi_{\mathbf{k}B}(\mathbf{0}) \approx \frac{1}{\sqrt{N}} \phi(\delta_1) \gamma_{\mathbf{k}}. \quad (\text{B3b})$$

The latter can be used in the expansion of  $\text{Re } G^0(\mathbf{x}, \mathbf{x}, \omega = 0)$  appearing in the resonance condition, Eq. (21), which for a site-like impurity reads

$$\begin{aligned} \text{Re } G^0(\mathbf{x}, \mathbf{x}, 0) &= \frac{s}{t} \sum_{\mathbf{k}\lambda} |\psi_{\mathbf{k}\lambda}(\mathbf{x})|^2 \\ &+ \frac{1}{t} \sum_{\mathbf{k}} \left( \frac{1}{\gamma_{\mathbf{k}}} \psi_{\mathbf{k}A}^*(\mathbf{x}) \psi_{\mathbf{k}B}(\mathbf{x}) + \text{H.c.} \right). \end{aligned} \quad (\text{B4})$$

Inserting Eqs. (B1) in Eq. (B4) and Eq. (21), one eventually obtains the estimate Eq. (22) for the impurity strength required to develop a resonance at  $\omega = 0$  in the site-like case.

A similar expansion holds in the bond-like and in the hollow-like cases, Eqs. (24) and (25), respectively involv-

ing the constants

$$A_b = -\frac{1}{N} \sum_{\mathbf{k}} \left( e^{i(\mathbf{k} \cdot \delta_3 - \theta_{\mathbf{k}})} + \text{H.c.} \right) \approx 0.67, \quad (\text{B5a})$$

$$A_h = \frac{1}{N} \sum_{\mathbf{k}} \left( e^{2i\theta_{\mathbf{k}}} \gamma_{\mathbf{k}} + \text{H.c.} \right) \approx 2.35, \quad (\text{B5b})$$

$$B_h = \frac{1}{N} \sum_{\mathbf{k}} |\gamma_{\mathbf{k}}|^2 = 3, \quad (\text{B5c})$$

where  $e^{i\theta_{\mathbf{k}}}$  is defined by Eq. (11).

### APPENDIX C: CURRENT DENSITY VECTOR WITHIN THE TIGHT-BINDING APPROXIMATION

Here, we summarize some of the results employed to derive the expression of the conductivity in Sec. IV B within the tight binding approximation outlined in Appendix B. We begin by reminding the explicit expression of the Fourier transform of the paramagnetic component of the density current vector in reciprocal space<sup>27</sup>

$$\tilde{\mathbf{J}}^{\nabla}(\mathbf{k}) = -\frac{e}{2m} \int \frac{d\mathbf{q}}{(2\pi)^2} (2\mathbf{q} + \mathbf{k}) c_{\mathbf{q}}^{\dagger} c_{\mathbf{k}+\mathbf{q}}. \quad (\text{C1})$$

In the homogeneous limit ( $\mathbf{k} = \mathbf{0}$ ), one has<sup>40</sup>

$$\tilde{\mathbf{J}}^{\nabla}(0) = \frac{e}{i\hbar} [H, \mathbf{r}], \quad (\text{C2})$$

where  $H$  is the system's Hamiltonian, including the impurity contribution. Exploiting Eq. (C2), one finds

$$\langle \mathbf{k}\alpha | \tilde{\mathbf{J}}^{\nabla}(0) | \mathbf{k}'\beta \rangle = ie \frac{ta}{\hbar} \delta_{\mathbf{k}', \mathbf{k}+\mathbf{G}} e^{i\mathbf{G} \cdot \delta_{\beta}} \mathbf{h}_{\alpha\beta}(\mathbf{k}), \quad (\text{C3})$$

where  $\alpha, \beta \in \{A, B\}$ ,  $\mathbf{G}$  is a vector of the reciprocal lattice, and  $\delta_{\beta} = \mathbf{0}$  if  $\beta = A$ , and  $\delta_{\beta} = \delta_3$  if  $\beta = B$ . Due to the discrete translational invariance and the hermiticity of the current density operator, the adimensional matrix elements  $\mathbf{h}_{\alpha\beta}(\mathbf{k})$  fulfill the additional properties

$$\mathbf{h}_{AA}(\mathbf{k}) = h_{BB}(\mathbf{k}), \quad (\text{C4a})$$

$$\mathbf{h}_{AA}(\mathbf{k}) = -h_{AA}(-\mathbf{k}), \quad (\text{C4b})$$

$$\mathbf{h}_{AB}(\mathbf{k}) = -h_{BA}(-\mathbf{k}). \quad (\text{C4c})$$

Moreover, the off-diagonal elements afford the explicit expression

$$\begin{aligned} \mathbf{h}_{AB}(\mathbf{k}) &= -\frac{i}{a} \nabla_{\mathbf{k}} \gamma_{\mathbf{k}} \\ &= \frac{1}{a} \sum_{\ell=1}^3 \delta_{\ell} e^{i\mathbf{k} \cdot \delta_{\ell}}, \end{aligned} \quad (\text{C5})$$

to leading order in the overlap parameter  $s$ , where use has been made of Eq. (5), which, together with Eq. (C4c), yields the off-diagonal terms of the matrix elements.

In order to find the diagonal terms, it is useful to observe that the pseudoatomic wavefunctions introduced in Appendix B are cylindrically symmetric. This implies the following overlap and dipole element for pseudoatomic wavefunctions centered on nearest neighbor sites

$$\int d\mathbf{r} \phi(\mathbf{r}) \phi(\mathbf{r} \pm \delta_{\ell}) = s, \quad (\text{C6a})$$

$$\int d\mathbf{r} \phi(\mathbf{r}) \mathbf{r} \phi(\mathbf{r} \pm \delta_{\ell}) = \mp \frac{1}{2} s \delta_{\ell}, \quad (\text{C6b})$$

where  $s$  is the band asymmetry parameter (Appendix B) and  $\ell = 1, 2, 3$ , or, more compactly,

$$\int d\mathbf{r} \phi(\mathbf{r}) \mathbf{r} \phi(\mathbf{r} - \mathbf{r}') = \frac{1}{2} \mathbf{r}' \int d\mathbf{r} \phi(\mathbf{r}) \phi(\mathbf{r} - \mathbf{r}'). \quad (\text{C6c})$$

Making use of Eq. (C6b), one eventually finds

$$\begin{aligned} \mathbf{h}_{\alpha\alpha}(\mathbf{k}) &= -\frac{i}{a} \frac{s}{2} \nabla_{\mathbf{k}} \beta_{\mathbf{k}} \\ &= \frac{s}{2a} \sum_{\ell=1}^3 \sum_{m=1, m \neq \ell}^3 (\delta_{\ell} - \delta_m) e^{i\mathbf{k} \cdot (\delta_{\ell} - \delta_m)}, \end{aligned} \quad (\text{C7})$$

with  $\beta_{\mathbf{k}}$  given by Eq. (B2).

\* Corresponding author. E-mail: giuseppe.angilella@ct.infn.it

<sup>1</sup> K. S. Novoselov, A. K. Geim, S. V. Morozov, D. Jiang, Y. Zhang, S. V. Dubonos, I. V. Grigorieva, and A. A. Firsov, *Science* **306**, 666 (2004).

<sup>2</sup> K. S. Novoselov, A. K. Geim, S. V. Morozov, D. Jiang, M. I. Katsnelson, I. V. Grigorieva, S. V. Dubonos, and A. A. Firsov, *Nature* **438**, 197 (2005).

<sup>3</sup> A. H. Castro Neto, F. Guinea, N. M. R. Peres, K. S.

Novoselov, and A. K. Geim, *Rev. Mod. Phys.* **81**, 000109 (2009).

<sup>4</sup> B. Uchoa, V. N. Kotov, N. M. R. Peres, and A. H. Castro Neto, *Phys. Rev. Lett.* **101**, 026805 (2008).

<sup>5</sup> Y. Zhang, Y. Tan, H. L. Stormer, and P. Kim, *Nature* **438**, 201 (2005).

<sup>6</sup> C. Berger, Z. Song, X. Li, X. Wu, N. Brown, C. Naud, D. Mayou, T. Li, J. Hass, A. N. Marchenkov, E. H. Conrad, P. N. First, and W. A. de Heer, *Science* **312**, 1191 (2006).



- <sup>7</sup> V. M. Pereira, F. Guinea, J. M. B. Lopes dos Santos, N. M. R. Peres, and A. H. Castro Neto, *Phys. Rev. Lett.* **96**, 036801 (2006).
- <sup>8</sup> V. V. Cheianov and V. I. Fal'ko, *Phys. Rev. Lett.* **97**, 226801 (2006).
- <sup>9</sup> C. Bena, *Phys. Rev. Lett.* **100**, 076601 (2008).
- <sup>10</sup> M. A. H. Vozmediano, M. P. López-Sancho, T. Stauber, and F. Guinea, *Phys. Rev. B* **72**, 155121 (2005).
- <sup>11</sup> N. M. R. Peres, F. Guinea, and A. H. Castro Neto, *Phys. Rev. B* **73**, 125411 (2006).
- <sup>12</sup> E. Stolyarova, K. T. Rim, S. Ryu, J. Maultzsch, P. Kim, L. E. Brus, T. F. Heinz, M. S. Hybertsen, and G. W. Flynn, *Proc. Nat. Acad. Sci.* **104**, 9209 (2007).
- <sup>13</sup> J. Martin, N. Akerman, G. Ulbricht, T. Lohmann, J. H. Smet, K. von Klitzing, and A. Yacoby, *Nat. Phys.* **4**, 144 (2008).
- <sup>14</sup> T. O. Wehling, A. V. Balatsky, M. I. Katsnelson, A. I. Lichtenstein, K. Scharnberg, and R. Wiesendanger, *Phys. Rev. B* **75**, 125425 (2007).
- <sup>15</sup> Y. V. Skrypnik and V. M. Loktev, *Phys. Rev. B* **75**, 245401 (2007).
- <sup>16</sup> D. M. Basko, *Phys. Rev. B* **78**, 115432 (2008).
- <sup>17</sup> M. Ishigami, J. H. Chen, W. G. Cullen, M. S. Fuhrer, and E. D. Williams, *Nano Lett.* **7**, 1643 (2007).
- <sup>18</sup> V. Geringer, M. Liebmann, T. Echtermeyer, S. Runte, M. Schmidt, R. Rückamp, M. C. Lemme, and M. Morgenstern, *Phys. Rev. Lett.* **102**, 076102 (2009).
- <sup>19</sup> P. Mallet, F. Varchon, C. Naud, L. Magaud, C. Berger, and J. Y. Veuillen, *Phys. Rev. B* **76**, 041403(R) (2007).
- <sup>20</sup> A. K. Geim and K. S. Novoselov, *Nature Mat.* **64**, 183 (2007).
- <sup>21</sup> E. H. Hwang, S. Adam, and S. Das Sarma, *Phys. Rev. Lett.* **98**, 186806 (2007).
- <sup>22</sup> K. I. Bolotin, K. J. Sikes, Z. Jiang, M. Klima, G. Fudenberg, J. Hone, P. Kim, and H. L. Stormer, *Solid State Commun.* **146**, 351 (2008).
- <sup>23</sup> Y. W. Tan, Y. Zhang, K. Bolotin, Y. Zhao, S. Adam, E. H. Hwang, S. Das Sarma, H. L. Stormer, and P. Kim, *Phys. Rev. Lett.* **99**, 246803 (2007).
- <sup>24</sup> T. Stauber, N. M. R. Peres, and A. H. Castro Neto, *Phys. Rev. B* **78**, 085418 (2008).
- <sup>25</sup> X. Du, I. Skachko, A. Barker, and E. Y. Andrei, *Nature Nanotech.* **3**, 491 (2008).
- <sup>26</sup> G. Forte, A. Grassi, G. M. Lombardo, A. La Magna, G. G. N. Angilella, R. Pucci, and R. Vilardi, *Phys. Lett. A* **372**, 6168 (2008).
- <sup>27</sup> H. Bruus and K. Flensberg, *Many-Body Quantum Theory in Condensed Matter Physics: An Introduction* (Oxford University Press, Oxford, 2004).
- <sup>28</sup> R. Saito, M. Fujita, G. Dresselhaus, and M. S. Dresselhaus, *Physical properties of carbon nanotubes* (Imperial College Press, London, 1998).
- <sup>29</sup> S. Reich, J. Maultzsch, C. Thomsen, and P. Ordejón, *Phys. Rev. B* **66**, 035412 (2002).
- <sup>30</sup> C. Bena, *Phys. Rev. B* **79**, 125427 (2009).
- <sup>31</sup> I. S. Gradshteyn and I. M. Ryzhik, *Table of Integrals, Series, and Products* (Academic Press, Boston, 1994), 5th ed.
- <sup>32</sup> V. M. Pereira, J. M. B. Lopes dos Santos, and A. H. Castro Neto, *Phys. Rev. B* **77**, 115109 (2008).
- <sup>33</sup> P. Esquinazi, D. Spemann, R. Höhne, A. Setzer, K. H. Han, and T. Butz, *Phys. Rev. Lett.* **91**, 227201 (2003).
- <sup>34</sup> J. B. Marston and I. Affleck, *Phys. Rev. B* **39**, 11538 (1989).
- <sup>35</sup> S. Chakravarty, R. B. Laughlin, D. K. Morr, and C. Nayak, *Phys. Rev. B* **63**, 094503 (2001).
- <sup>36</sup> J. X. Zhu, W. Kim, C. S. Ting, and J. P. Carbotte, *Phys. Rev. Lett.* **87**, 197001 (2001).
- <sup>37</sup> D. K. Morr, *Phys. Rev. Lett.* **89**, 106401 (2002).
- <sup>38</sup> N. Andrenacci, G. G. N. Angilella, H. Beck, and R. Pucci, *Phys. Rev. B* **70**, 024507 (2004).
- <sup>39</sup> M. Trushin and J. Schliemann, *Europhys. Lett.* **83**, 17001 (2008).
- <sup>40</sup> I. Paul and G. Kotliar, *Phys. Rev. B* **67**, 115131 (2003).